Bouncing droplet dynamics above the Faraday threshold

Bouncing droplet dynamics above the Faraday threshold

L. D. Tambasco, J. J. Pilgram, and J. W. M. Bush

Citation: Chaos **28**, 096107 (2018); doi: 10.1063/1.5031426
View online: https://doi.org/10.1063/1.5031426
View Table of Contents: http://aip.scitation.org/toc/cha/28/9
Published by the American Institute of Physics

Bouncing droplet dynamics above the Faraday threshold

L. D. Tambasco,[1] J. J. Pilgram,[2] and J. W. M. Bush[1,a)]
[1]*Department of Mathematics, Massachusetts Institute of Technology, Cambridge, Massachusetts 02139, USA*
[2]*Department of Physics, California Polytechnic State University, San Luis Obispo, California 93407, USA*

(Received 29 March 2018; accepted 24 August 2018; published online 14 September 2018)

We present the results of an experimental investigation of the dynamics of droplets bouncing on a vibrating fluid bath for forcing accelerations above the Faraday threshold. Two distinct fluid viscosity and vibrational frequency combinations (20 cS–80 Hz and 50 cS–50 Hz) are considered, and the dependence of the system behavior on drop size and vibrational acceleration is characterized. A number of new dynamical regimes are reported, including meandering, zig-zagging, erratic bouncing, coalescing, and trapped regimes. Particular attention is given to the regime in which droplets change direction erratically and exhibit a dynamics akin to Brownian motion. We demonstrate that the effective diffusivity increases with vibrational acceleration and decreases with drop size, as suggested by simple scaling arguments. *Published by AIP Publishing.* https://doi.org/10.1063/1.5031426

A droplet may walk on the surface of a vertically vibrated fluid bath, propelled by the waves generated by its previous impacts. The resulting hydrodynamic pilot-wave system exhibits several features that were once thought to be peculiar to quantum systems. To date, attention has primarily been restricted to the dynamics of droplets below the Faraday threshold, the critical vibrational acceleration above which the interface becomes unstable in the absence of drops. We here examine the droplet dynamics arising above the threshold. Specifically, we characterize the dependence of the droplet behavior on the drop size and vibrational acceleration and so develop a pair of regime diagrams for two different combinations of fluid viscosity and vibrational frequency. We give particular focus to the erratic bouncing regime, where the drop executes Brownian motion. In this regime, we characterize the dependence of the effective diffusivity on droplet radius and vibrational acceleration.

I. INTRODUCTION

Droplets walking on a vibrating fluid bath have been shown to exhibit several features of quantum mechanical systems,[1] including quantized orbits,[2–5] tunneling,[6,7] and the emergence of multimodal statistics in confined geometries.[8,9] Walking droplets are an example of a pilot-wave system: the droplet generates a wave at every impact with the bath and is, in turn, guided by the local slope of the bath surface, whose form is prescribed by the superposition of waves generated from previous bounces. The longevity of the waves is controlled by the vibrational acceleration of the bath, γ. If $\gamma < \gamma_F$, where γ_F is the Faraday threshold, the surface would remain unperturbed in the absence of the drop.[10] As γ approaches γ_F from below, linear waves generated by the drop persist for the memory time $T_M = T_d/(1-\gamma/\gamma_F)$, where $T_d \sim \lambda_F^2/\nu$ is the temporal decay time of the waves in the absence of forcing.[11] Nonlinear wave effects are expected to be important near the Faraday threshold. For $\gamma > \gamma_F$, the entire surface becomes unstable to the Faraday instability so that waves appear throughout the bath. In previous experimental investigations of this hydrodynamic pilot-wave system, care was taken to ensure that γ remained below γ_F, thus avoiding the appearance of a background Faraday wavefield and ensuring that the drop was guided solely by its pilot-wave field. For $\gamma < \gamma_F$, the walking drops execute rectilinear motion provided they are sufficiently far from boundaries.[12,13]

Stochastic electrodynamics is a sub-branch of quantum field theory, according to which microscopic quantum particles interact with a background field, specifically zero-point electromagnetic vacuum fluctuations.[16] Notably, the inferred energy spectrum of this zero-point field $E(\omega) = \hbar\omega/2$ allows for the introduction of Planck's constant, $\hbar$, into a classical theory.[14] The zero-point field has been sought as the basis for an electromagnetic pilot-wave theory in quantum mechanics,[15,16] in which case it would play the role of the vibrating bath in the hydrodynamic pilot-wave system in energizing the system.[1] Stochastic dynamics,[17,18] de Broglie's pilot-wave theory,[19] and Bohmian mechanics[20] have all likewise sought to rationalize quantum mechanics in terms of interactions between microscopic particles and a stochastic background field. With a view to introducing an irregular forcing into this hydrodynamic pilot-wave system and so exploring a regime that might potentially yield new hydrodynamic quantum analogs, we were thus compelled to examine the dynamics of bouncing droplets interacting with a background field consisting of the Faraday wavefield arising for $\gamma > \gamma_F$. Our study thus represents a variant of the bouncing ball dynamics that has been explored extensively in the dynamical systems community.[21,22]

In the hydrodynamic pilot-wave system, the waves serve to propel the bouncing drops by imparting an impulse during impact. If the vertical dynamics of the droplet are aperiodic, that is, the phase of impact relative to the Faraday wave changes with every bounce, then the resulting lateral impulses will be irregular. These impulses are thus expected to serve as a source of stochasticity in hydrodynamic pilot-wave systems and so may give rise to new dynamical states. For example, Oza *et al.*[23]

a)bush@math.mit.edu

theoretically demonstrated that self-orbiting states exist but are unstable for accessible fluid parameters below the Faraday threshold. The role of noise in the stability of hydrodynamic spin states has also been examined.[24] The question naturally arises as to whether these spin states might exist above the Faraday threshold, where the confining wave force required for stable spin states might be amplified.

Prior studies examined droplets bouncing above the Faraday threshold in two specific cases. First, Sampara and Gilet explored the dynamics of bouncing droplets on a bath forced by two frequencies.[25] Second, Sungar *et al.*[26] introduced an array of pillars to the bath and observed that, for $\gamma/\gamma_F \simeq 1.02$, the form of the Faraday waves in the vicinity of the pillars is analogous to that arising in the optical Talbot effect.[27] The resulting Faraday-Talbot wave pattern was capable of trapping both walking and bouncing droplets in its troughs, a hydrodynamic analog of particle trapping with the Talbot effect.[28,29] We here characterize the dynamics of droplets above the Faraday threshold in the absence of pillars, forced with a single frequency, and identify the regimes where droplets become trapped by the underlying Faraday wavefield.

The bouncing and walking behavior of drops on a bath vibrating below the Faraday threshold have been thoroughly characterized experimentally,[11,30,31] and considerable effort has been devoted to rationalizing this behavior theoretically.[5,12,32–34] We here extend the regime diagrams of Wind-Willassen *et al.*[12] for silicone oil droplets of kinematic viscosity 20 and 50 cSt at driving frequencies of 80 and 50 Hz, respectively. In Sec. II, we describe our experimental apparatus and methods. In Sec. III, we enumerate the dynamic states arising above the Faraday threshold. In Sec. IV, we examine the dynamics of drops bouncing erratically above the Faraday threshold, demonstrating that they exhibit behavior akin to a two-dimensional random walk. We then characterize the dependence of the effective drop diffusivity on droplet size and forcing acceleration, and rationalize this dependence via simple scaling arguments.

II. EXPERIMENTS

We explore the bouncing and walking dynamics above the Faraday threshold in a circular bath filled to a depth of $h = 6$ mm with silicone oil of viscosity $\nu = 20$ or 50 cS. A schematic of the experimental arrangement is presented in Fig. 1. The bath is vibrated vertically with amplitude A, frequency f, and acceleration $\Gamma(t) = \gamma\cos(2\pi ft)$, where $\gamma = A(2\pi f)^2$. Two vibrational frequencies are considered, $f = 50$ Hz for the 50 cS oil and $f = 80$ Hz for the 20 cS oil, the combinations considered below threshold in prior work.[12,30,32] When the vibrational acceleration is sufficiently large, $\gamma > \gamma_F$, the surface of the bath becomes unstable to subharmonic Faraday waves that oscillate with frequency $f/2$ and wavelength $\lambda_F = 2\pi/k_F$. The observed wave-number k_F is well described by the standard water-wave dispersion relation

$$\omega_F^2(k) = \left(gk + \frac{\sigma}{\rho}k^3\right)\tanh(kh), \tag{1}$$

where $\omega_F = \omega/2 = \pi f$ is the subharmonic angular frequency, g the gravitational acceleration, σ the surface tension, and

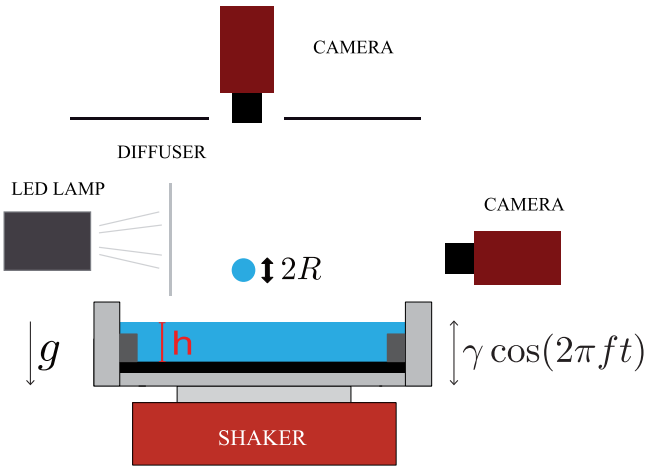

FIG. 1. Experimental arrangement.[35] The fluid bath is shaken using an electromagnetic shaker coupled with an air bearing that constrains the vibrations to be vertical. A CCD camera placed above the bath captures the horizontal dynamics, and a high-speed Phantom camera allows for resolution of the vertical dynamics.

ρ the fluid density. For the depth considered, $h = 6$ mm, a vibrational frequency $f = 80$ Hz corresponds to a Faraday wavelength $\lambda_F = 4.75$ mm, and 50 Hz to $\lambda_F = 6.98$ mm.

While the wavelength is prescribed by Eq. (1), the wave pattern realized depends on both container shape and vibrational acceleration. For our circular bath, the most unstable mode at the onset of the Faraday instability, $\gamma \simeq \gamma_F$, is a boundary-dominated circularly-symmetric wave, with crests arranged in concentric rings separated by λ_F [Fig. 2(a)]. As the forcing acceleration γ is increased beyond approximately $1.015\gamma_F$, the circularly symmetric wavefield is replaced by a checkerboard pattern with characteristic spacing λ_F [Fig. 2(b)]. In this regime, the boundary geometry has effectively no influence on the background field of Faraday waves. Successive instabilities arising as γ increases progressively beyond γ_F have been characterized by Douady.[36] At the highest forcing acceleration considered in our study, $\gamma/\gamma_F = 1.2$, the background wavefield consisted of a standing checkerboard pattern.

When the vibrational acceleration is sufficiently large, the interface breaks [Fig. 2(c)]. The critical acceleration for surface rupture in a vertically vibrating bath has been determined empirically and theoretically.[37,38] For low viscosity fluids, the interface breaks when the upward inertial force due to the vibrational acceleration $\gamma \sim 4g$ exceeds the stabilizing force associated with surface tension: $m\gamma > 2\pi\lambda_F\sigma$, where $m \sim \rho\lambda_F^3$ is the accelerated fluid mass. Using the dispersion relation for deep-water capillary waves for λ_F yields the critical acceleration γ_R for interfacial rupture,

$$\gamma_R = C\left(\frac{\sigma}{\rho}\right)^{1/3}\omega^{4/3}, \tag{2}$$

where C is an $\mathcal{O}(1)$ constant that depends on the fluid-frequency combination. For 20 cS silicone oil vibrated at 80 Hz, $\gamma_R/\gamma_F \approx 4.02$, while for 50 cS oil vibrated at 50 Hz, $\gamma_R/\gamma_F \approx 2.15$. When γ_R is exceeded, the system is characterized by continuous droplet creation and annihilation,

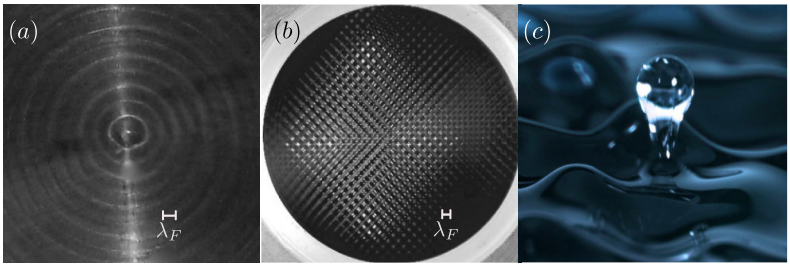

FIG. 2. (a) Circularly-symmetric Faraday pattern arising at the onset of the Faraday instability, $\gamma/\gamma_F \approx 1.01$. (b) Checkerboard Faraday pattern emerging at $\gamma/\gamma_F = 1.05$. (c) Faraday wave rupture generates drops when the vibrational acceleration is sufficiently high, $\gamma > \gamma_R$ ($= 4.02\gamma_F$ for 20 cS oil vibrated at 80 Hz).

specifically, coalescence with the bath. As γ_R was not accessible with our experimental apparatus, we simply state it as a bound above which one may no longer consider the motion of single drops.

In order to characterize the droplet dynamics above the Faraday threshold, we use a piezo-electric droplet generator[39] to repeatably create drops of uniform radii R in the range $0.2\,\text{mm} < R < 0.5\,\text{mm}$ (with $\pm 0.5\%$ variability). We generate a single drop, place it at the center of the domain, and then affix a circular acrylic lid on top of the bath to eliminate the influence of air currents. We gradually increase the forcing acceleration beyond the Faraday threshold, $\gamma > \gamma_F$. A CCD camera placed above the bath captures the horizontal motion of the drop. A light-emitting diode (LED) lamp and diffuser illuminate the setup from the side while a high-speed Phantom camera placed beside the bath captures the vertical dynamics, also allowing for accurate measurement of the drop radius.

We sweep through the forcing accelerations above the Faraday threshold, $\gamma/\gamma_F > 1$, at increments $\Delta\gamma/\gamma_F = 0.001$ for drops with radii in the range $0.1\,\text{mm} < R < 0.5\,\text{mm}$, corresponding to non-dimensional vibration numbers $\Omega \equiv \omega/\sqrt{\sigma/(\rho R^3)}$ in the range $[0.1, 1.2]$. For each value of the forcing acceleration, we record the trajectory of the drop for one minute, or until it reaches the edge of the circular bath. We use the recordings to characterize the dynamics, as will be summarized in Sec. III.

We characterize droplet trajectories in terms of a persistence length L_p,[40] defined as

$$\langle \cos\theta \rangle = e^{-s/L_p}, \tag{3}$$

where θ is the angle between the tangent velocity vectors at an initial point and at another point an arclength s further along the trajectory. $\langle\cdot\rangle$ indicates the average value over all initial points along a single trajectory. Similar measures of coherence have been used by Gilet[41] in his study of chaotic walker motion in corrals below the Faraday threshold. The relative magnitudes of L_p, the characteristic length over which the drop changes direction, and the Faraday wavelength λ_F provides a quantitative means of classifying the coherence of the trajectories through the non-dimensional persistence length $\Lambda = L_p/\lambda_F$. We note that the persistence length typically varies between individual trajectories, but its characteristic value is nevertheless valuable in classifying the system behavior into different regimes.

III. RESULTS

We summarize the observed droplet dynamics above the Faraday threshold for 20 cS silicone oil driven at 80 Hz in the regime diagram shown in Fig. 3(a). For all driving accelerations above γ_F, the smallest drops ($R < 0.2\,\text{mm}$, corresponding to $\Omega < 0.31$) tend to bounce irregularly, moving erratically in the horizontal until eventually coalescing. We note that similar behavior also arises for these drops below the Faraday threshold.[32]

Slightly larger drops ($0.2\,\text{mm} < R < 0.4\,\text{mm}$ or $0.31 < \Omega < 0.86$) walk along straight paths below γ_F. For $\gamma > \gamma_F$, they follow meandering trajectories, such as that shown in Fig. 4(a), characterized by a relatively large non-dimensional persistence length, $1 < \Lambda < 2$. In this regime, the amplitude

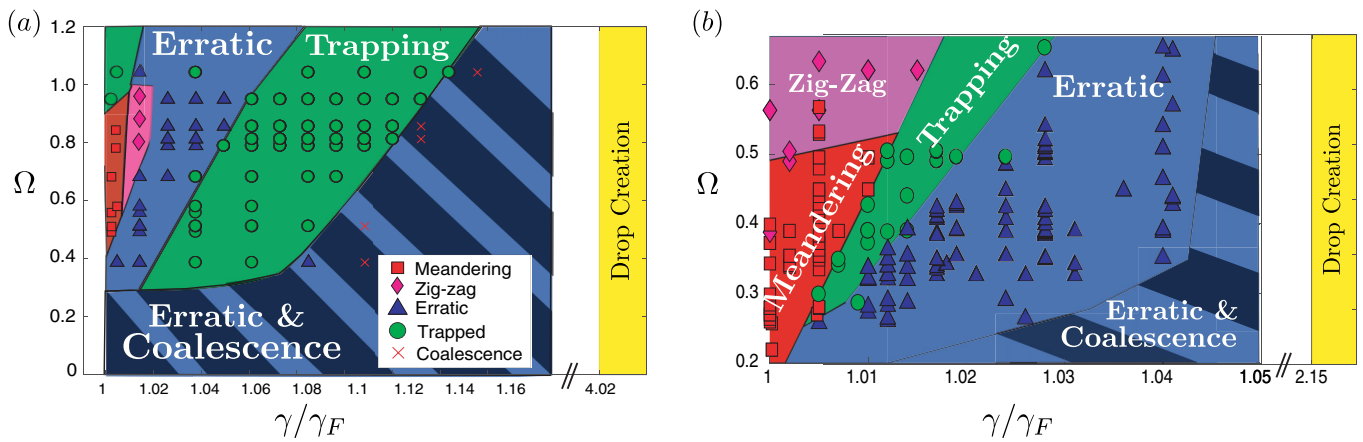

FIG. 3. Regime diagrams indicating the behavior of drops levitated on a vibrating bath for $\gamma/\gamma_F > 1$. We delineate the parameter regimes as a function of the dimensionless forcing acceleration γ/γ_F and vibration number $\Omega = \omega/\sqrt{\sigma/(\rho R^3)}$. (a) 20 cS silicone oil driven at 80 Hz and (b) 50 cS silicone oil driven at 50 Hz. The meandering regime is indicated in red, zig-zagging in pink, erratic bouncing in blue, trapping in green, and coalescing in striped black/blue regions. Yellow indicates the regime of spontaneous drop creation from breaking Faraday waves, as arises when the forcing acceleration exceeds the threshold for interface rupture ($\gamma > \gamma_R$). Note the difference in horizontal scales between panels (a) and (b).

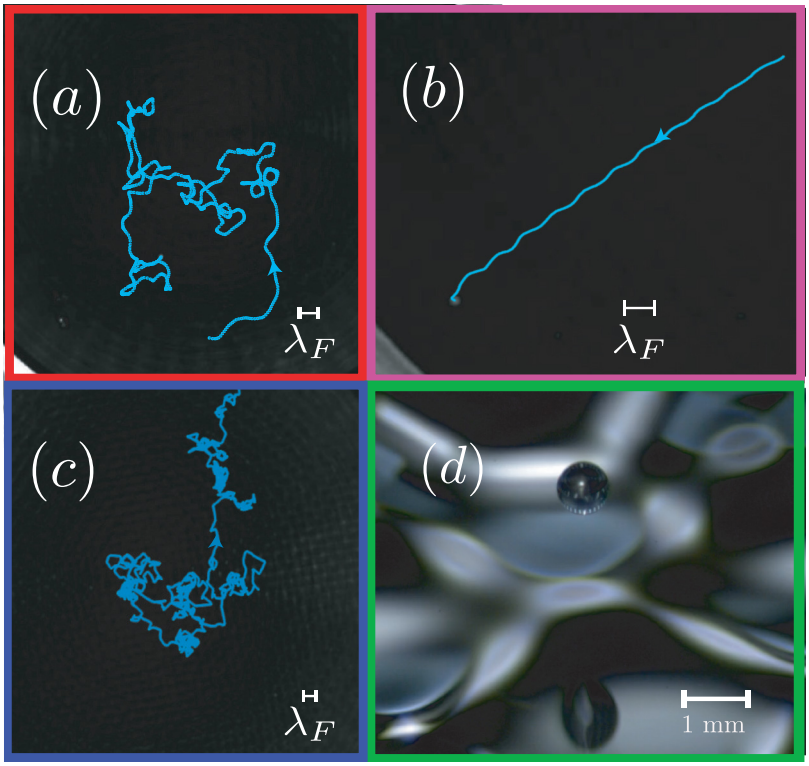

FIG. 4. Dynamic states observed for $\gamma > \gamma_F$. (a) Meandering trajectory, characterized by a persistence length greater than the Faraday wavelength, $\Lambda = L_p/\lambda_F > 1$. For this particular trajectory, $\Lambda = 1.15$. (b) A zig-zagging trajectory is characterized by small amplitude lateral oscillations, with wavelength on the order of λ_F, along a mean rectilinear trajectory. The drop navigates the crests and troughs of the underlying checkerboard Faraday wave pattern. (c) Erratic walking, characterized by a dimensionless persistence length $\Lambda < 1$. For this particular trajectory, $\Lambda = 0.24$. (d) Side view of a droplet trapped above the Faraday threshold in a (4,1) bouncing mode. The drop bounces in place on the trough of the underlying subharmonic wave once every 4 driving periods (with period $2T_F$).

of the Faraday wavefield is small relative to the drop's pilot-wave, so only weakly alters the walker's direction. We note also that small loops of radius $\lambda_F/2$ were often apparent in meandering trajectories [Fig. 4(c)], indicating a tendency toward hydrodynamic spin states.[23,24] However, the underlying wavefield is still insufficient to stabilize these spin states: in the parameter regime considered, the loops were always transient, never stable.

As the forcing acceleration is further increased ($\gamma/\gamma_F \sim 1.015$), meandering gives way to relatively regular zig-zagging trajectories, as shown in Fig. 4(b), a transition that coincides with the emergence of a checkerboard Faraday pattern on the fluid surface [Fig. 2(b)]. In zig-zagging trajectories, the drop slightly deviates from a straight-line path, with oscillations perpendicular to its direction of mean motion. The oscillations occur with a characteristic wavelength on the order of λ_F, indicating that the drop is navigating the background checkerboard field of Faraday waves.

For $1.015 \lesssim \gamma/\gamma_F \lesssim 1.04$, the amplitude of the underlying Faraday wave becomes comparable to or larger than that of the pilot-wave generated by the drop, and the droplet motion becomes highly irregular [see Fig. 4(c)]. Due to the loss of resonance in the vertical dynamics, each impact arises at a different phase, so the drop impacts a different waveform at every bounce. Since the drop's horizontal motion is driven by the gradient of the underlying wave, it changes direction in response to these varying impulses on the time scale of its characteristic bouncing period T_F. The frequent change of direction translates to a dimensionless persistence length less than 1, typically in the range $0.1 < \Lambda < 0.5$, allowing for differentiation from the meandering trajectories arising at lower γ/γ_F.

For $\gamma/\gamma_F \gtrsim 1.04$, the checkerboard pattern is able to trap droplets of a certain size, causing them to bounce in place indefinitely in the absence of external perturbations. A trapped droplet is shown in Fig. 4(d); the droplet bounces periodically in a (4,1) bouncing mode, once every 4 driving periods.[42] We note also that the trapping is relatively robust; perturbations to trapped states cause the drop to move erratically for a few seconds of transient motion before being trapped in another trough. In this regime, the disturbance generated by the drop impact is typically one tenth the amplitude of the underlying Faraday wavefield. The relative amplitude of the background and drop-generated wavefields is clearly a key parameter in studying drop motion above the Faraday threshold.

A further increase in forcing acceleration ($\gamma/\gamma_F \gtrsim 1.12$) leads to longer transients thereby increasing the likelihood of drop coalescence. Finally, the largest drops considered ($R > 0.45$ mm, or $\Omega > 0.86$) tend to bounce in place at the onset of the Faraday threshold, but then undergo similar transitions, from erratic motion to trapping, and eventually erratic bouncing and coalescence.

Figure 3(b) shows the regime diagram for 50 cS oil driven at 50 Hz above the Faraday threshold. The observed dynamical states are similar to those observed for the 20 cS–80 Hz viscosity-frequency combination, but the transitions happen over a significantly smaller range of forcing accelerations, as is evident in the different horizontal axis scales of Figs. 3(a) and 3(b). We note that the range of droplet sizes that can be levitated in this parameter regime is smaller. Below the Faraday threshold, all droplets are walkers in the drop size range considered. Just above the threshold, smaller droplets ($R < 0.38$ mm, $\Omega < 0.50$) meander, while larger drops ($R > 0.38$ mm, $\Omega > 0.50$) zig-zag. Stable droplet

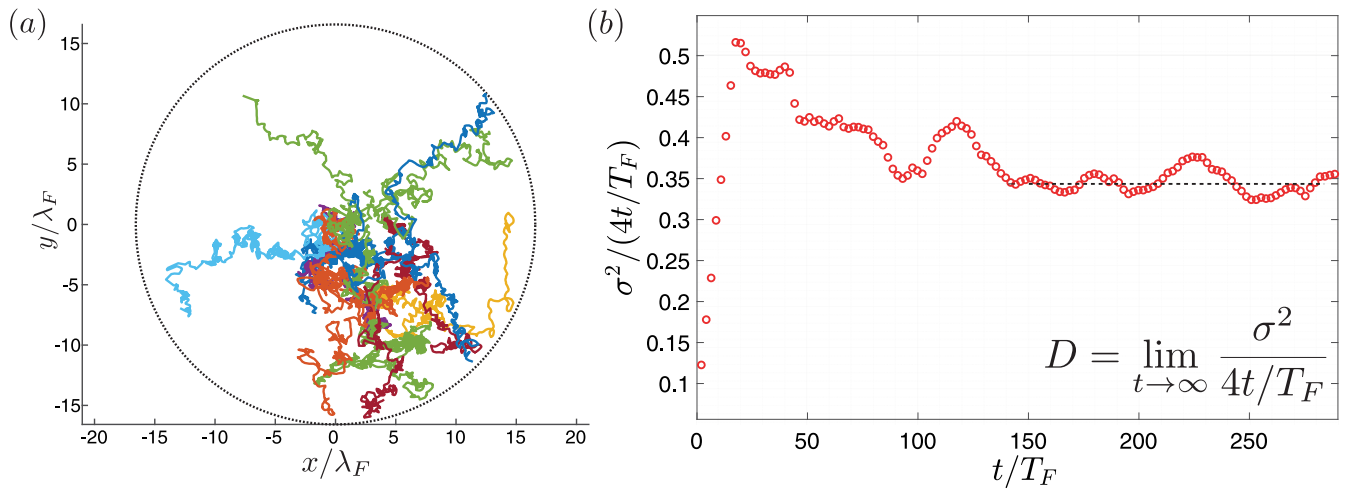

FIG. 5. (a) Erratic trajectories resembling two-dimensional Brownian motion for droplets of radius $R = 0.376$ mm vibrated at $\gamma/\gamma_F = 1.01$, corresponding to the erratic regime in Fig. 3(a). The circle indicates the boundary of the bath. (b) The effective diffusivity D for the trajectories in Fig. 5(a) may be computed from the long-time limit of the mean-squared displacement scaled by the non-dimensional time $4t/T_F$. The initial phase of ballistic diffusion (for $t \leq 15T_F$) is a transient effect resulting from the drop being initialized in a free walking state (at $\gamma < \gamma_F$).

trapping is observed over a narrow range of forcing accelerations ($1.005 \lesssim \gamma/\gamma_F \lesssim 1.02$). For larger γ, trapping states become unstable, giving rise to erratic bouncing. Drops of all sizes eventually coalesce for $\gamma/\gamma_F \gtrsim 1.04$. Spontaneous droplet creation through interfacial fracture occurs for $\gamma > \gamma_R = 2.15\gamma_F$.

IV. 2D EFFECTIVE DIFFUSION

Brownian motion may be characterized in terms of a diffusion coefficient,

$$D = \lim_{t\to\infty} \frac{\sigma^2(t)}{4t}, \tag{4}$$

where $\sigma^2(t)$ is the variance in position, or mean-squared displacement, of many realizations of the associated random walk as a function of time. We can thus compute the effective diffusivity in the erratic bouncing (blue) region in Fig. 3. For each combination of droplet size and forcing acceleration, we recorded 10 trajectories such as those shown in Fig. 5(a) and calculated the corresponding mean-squared displacement, which is shown to scale linearly with time in the long-time limit [Fig. 5(b)]. We take the last 100 values of the mean-squared displacement and use their mean to obtain the effective diffusivity and their standard deviation for error bars.

Over the relatively small parameter regime of interest (see Fig. 3), the effective diffusivity depends only weakly on forcing acceleration and droplet size. As γ increases, the diffusion process is slightly enhanced, as suggested by Fig. 6(a). Similarly, Fig. 6(b) suggests that smaller drops tend to diffuse slightly faster than larger drops. We proceed by obtaining a rough scaling argument for the dependence of diffusivity on drop size and forcing acceleration by modeling the impact of the droplet with the bath using a linear spring[32] with a spring constant proportional to the surface tension σ.[42] A drop of radius R and mass $m = 4\rho\pi R^3/3$ will have characteristic speed $v \propto \sqrt{\sigma/\rho R}$ after impact, assuming a penetration depth $\Delta z \sim R$. The horizontal component of the drop's velocity v_x depends on the slope of the surface, which scales as $\eta/\lambda_F \sim \sqrt{(\gamma/\gamma_F - 1)}$ due to the supercritical bifurcation at the onset of the Faraday instability;[43] thus,

$$v_x \sim \sqrt{\frac{\sigma}{\rho R}}\frac{\eta}{\lambda_F} \sim \sqrt{\frac{\sigma(\gamma/\gamma_F - 1)}{\rho R}}. \tag{5}$$

Over one bounce, the droplet will traverse a characteristic distance $\Delta x = v_x T_F$. Since the drop is changing directions frequently in the erratic regime, on the time scale of the bouncing, the characteristic time scale of direction change

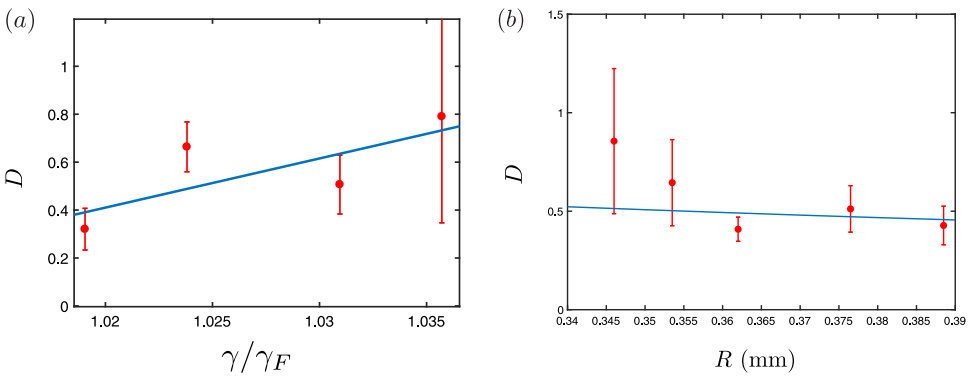

FIG. 6. The observed dependence of the effective diffusion coefficient D on (a) the forcing acceleration γ/γ_F for a drop of radius $R = 0.376$ mm and (b) the droplet radius R for $\gamma/\gamma_F = 1.031$. Dashed curves correspond to the effective diffusivity obtained from scaling arguments, Eq. (6). We note that surface diffusion arises in a relatively narrow region of parameter space ($1.015 \lesssim \gamma/\gamma_F \lesssim 1.04$) for 20 cS–80 Hz configuration as shown in Fig. 3(a), so only small variations in the effective diffusivity are apparent.

$\Delta t = T_F$, yielding a scaling for the effective diffusivity

$$D \equiv \frac{(\Delta x)^2}{\Delta t} = v_x^2 T_F \sim \frac{\sigma T_F}{\rho R}\left(\gamma/\gamma_F - 1\right). \tag{6}$$

The weak trends, evident in Fig. 6, of D increasing with the distance from threshold $(\gamma/\gamma_F - 1)$ and decreasing with radius R are both consistent with this simple scaling. While these trends are barely discernible over the limited parameter regime accessible in the systems considered, they may have some bearing in a more general pilot-wave setting.

V. DISCUSSION AND CONCLUSIONS

We have expanded the characterization of bouncing and walking droplet dynamics, extending the regime diagrams for 20 cS–80 Hz and 50 cS–50 Hz configurations above the Faraday threshold. We classified the droplet dynamics into the following regimes: trapped, coalescing, zig-zagging, meandering, and erratic bouncing. The meandering and erratic bouncing regimes were differentiated on the basis of the dimensionless persistence length $\Lambda = L_p/\lambda_F$. At the onset of the Faraday instability, while the drop's pilot-wave is still comparable in amplitude to the unstable background Faraday wave, coherent motion (zig-zagging or meandering) arises, characterized by a dimensionless persistence length $\Lambda \gtrsim 1$. As the forcing acceleration is increased further, the background Faraday wavefield dominates the pilot-wave, causing the drop to change directions more frequently and abruptly so that $0.1 < \Lambda < 0.5$. The impact of the relative contribution of the pilot-wave and the background Faraday wavefield on drop dynamics in different geometric settings is a subject of current interest. For example, we have recently considered the interaction of a walker and the wavefield generated by a circular well, assessing the ability of the well-induced waves to trap walkers.[44]

In Fig. 7, we summarize our results in a regime diagram for levitating drops of 20 cS oil driven at 80 Hz that combines Fig. 3(a) with the regime diagram presented in Fig. 11(d) of Molácek and Bush.[33] We note that the meandering and zig-zagging regimes are a continuous extension of the walking regime observed below the Faraday threshold. Likewise, the erratic bouncing and coalescing regime arising for smaller drops is simply a continuation of that below the threshold. We note that the boundaries of the regime diagram are determined empirically. The form of previous regime diagrams was rationalized through consideration of the dynamic interaction between the bouncing drop and its wavefield.[12,32,33] Below γ_F, the wave forms may be described in terms of a superposition of linear waves, an assumption that breaks down at and above the Faraday threshold. While providing theoretical rationale for the behavior for $\gamma > \gamma_F$ is thus not straightforward, it is hoped that our study may serve to motivate and guide further theoretical developments.

We have further characterized the emergence of Brownian motion above the Faraday threshold. In the erratic regime, when the bouncing of the drop is not synchronized with the Faraday wave, the force imparted by the bath changes at every impact in both magnitude and direction. This asynchrony introduces an irregular component into the drop's trajectory, leading to motion that may be described in terms of classical diffusion. While the diffusivity varies weakly over the limited parameter regime accessible, we infer that it is proportional to the forcing acceleration and inversely proportional to the drop size, as suggested by simple scaling arguments. We note that in a recent study, Hubert *et al.*[45] have simulated and characterized diffusive walker behavior below the Faraday threshold. Such diffusive-like behavior has also been reported for walkers in corrals below the Faraday threshold.[8,41,46]

If unperturbed by boundaries or applied forces, a walker at $\gamma < \gamma_F$ executes rectilinear motion at its free walking speed. This simple base state might be taken as a shortcoming of the walker system as a quantum analog system if one assumes that quantum particles diffuse in some fashion. However, the solution of the time-dependent linear Schrödinger equation for the probability density of a single free particle initially localized to the extent possible given Heisenberg's uncertainty relation, $\Delta p \Delta x \geq \hbar/2$, indicates ballistic diffusion, for which the variance $\sigma^2 \sim t^2$. This solution is thus consistent with the rectilinear motion of an ensemble of quantum particles with initial positions and momentum distributions prescribed by the uncertainty relations. According to the ensemble or statistical interpretation of quantum mechanics,[47] quantum diffusion may thus be simply understood as resulting from the uncertainty of the particle's initial conditions.[18] The walker's base state of rectilinear motion is thus not necessarily a shortcoming of the system as a hydrodynamic quantum analog, and its free walking velocity should be taken as the analog of $\hbar\mathbf{k}/m$. It remains an open question as to whether a stochastic forcing needs to be invoked in the walker system to capture certain features of quantum mechanics, or whether chaotic pilot-wave dynamics will be sufficient.

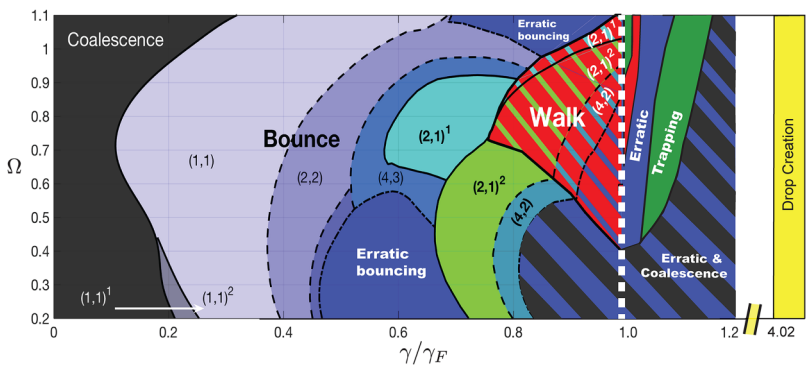

FIG. 7. An extension of the regime diagram obtained by Molácek and Bush[33] for 20 cS silicone oil driven at 80 Hz, including droplet dynamics above the Faraday threshold, as reported in Fig. 3(a). We delineate the parameter regimes as a function of the dimensionless forcing acceleration γ/γ_F and vibration number $\Omega = \omega/\sqrt{\sigma/(\rho R^3)}$. Walkers transition into the meandering and zig-zagging regimes. Small erratic bouncers ($R < 0.2$ mm, $\Omega < 0.31$) tend to coalesce just above the Faraday threshold, while large bouncers ($R > 0.45$ mm, $\Omega > 0.86$) tend to drift until being trapped.

ACKNOWLEDGMENTS

This work was supported by the U.S. National Science Foundation through Grant Nos. DMS-1614043 and CMMI-1727565. J.J.P. was supported through the MIT Summer Research Program. The authors would like to thank Giuseppe Pucci for valuable discussion and experimental assistance.

[1]J. W. M. Bush, "Pilot-wave hydrodynamics," Annu. Rev. Fluid Mech. **47**, 269–292 (2015).
[2]E. Fort, A. Eddi, A. Boudaoud, J. Moukhtar, and Y. Couder, "Path-memory induced quantization of classical orbits," Proc. Natl. Acad. Sci. **107**, 17515–17520 (2010).
[3]D. M. Harris and J. W. M. Bush, "Droplets walking in a rotating frame: From quantized orbits to multimodal statistics," J. Fluid Mech. **739**, 444–464 (2014).
[4]S. Perrard, M. Labousse, M. Miskin, E. Fort, and Y. Couder, "Self-organization into quantized eigenstates of a classical wave-driven particle," Nat. Commun. **5**, 3219 (2014).
[5]M. Durey and P. A. Milewski, "Faraday wave–droplet dynamics: Discrete-time analysis," J. Fluid Mech. **821**, 296–329 (2017).
[6]A. Eddi, E. Fort, F. Moisy, and Y. Couder, "Unpredictable tunneling of a classical wave-particle association," Phys. Rev. Lett. **102**, 240401 (2009).
[7]A. Nachbin, P. A. Milewski, and J. W. M. Bush, "Tunneling with a hydrodynamic pilot-wave model," Phys. Rev. Fluids **2**, 034801 (2017).
[8]D. M. Harris, J. Moukhtar, E. Fort, Y. Couder, and J. W. M. Bush, "Wave-like statistics from pilot-wave dynamics in a circular corral," Phys. Rev. E **88**, 011001 (2013).
[9]P. J. Sáenz, T. Cristea-Platon, and J. W. M. Bush, "Statistical projection effects in a hydrodynamic pilot-wave system," Nat. Phys. **14**, 315 (2017).
[10]T. B. Benjamin and F. Ursell, "The stability of the plane free surface of a liquid in vertical periodic motion," Proc. R. Soc. A **225**, 505–515 (1954).
[11]A. Eddi, E. Sultan, J. Moukhtar, E. Fort, M. Rossi, and Y. Couder, "Information stored in Faraday waves: The origin of path memory," J. Fluid Mech. **675**, 433–463 (2011).
[12]Ø. Wind-Willassen, J. Moláček, D. M. Harris, and J. W. M. Bush, "Exotic states of bouncing and walking droplets," Phys. Fluids **25**, 082002 (2013).
[13]G. Pucci, D. M. Harris, L. M. Faria, and J. W. M. Bush, "Walking droplets interacting with single and double slits," J. Fluid Mech. **835**, 1136–1156 (2018).
[14]T. H. Boyer, "Any classical description of nature requires classical electromagnetic zero-point radiation," Am. J. Phys. **79**, 1163–1167 (2011).
[15]L. de la Peña and A. M. Cetto, *The Quantum Dice: An Introduction to Stochastic Electrodynamics* (Springer Science and Business Media, Dordrecht, 1996).
[16]L. de la Peña, A. Cetto, and A. Hernández, *The Emerging Quantum: The Physics Behind Quantum Mechanics* (Springer International Publishing, 2014).
[17]E. Nelson, "Review of stochastic mechanics," J. Phys. Conf. Ser. **361**, 012011 (2012).
[18]G. Grössing, S. Fussy, J. M. Pascasio, and H. Schwabl, "Elements of sub-quantum thermodynamics: Quantum motion as ballistic diffusion," J. Phys. Conf. Ser. **306**, 012046 (2011).
[19]L. de Broglie, "Interpretation of quantum mechanics by the double solution theory," Ann. Fond. Louis Broglie **12**(4), 1–23 (1987).
[20]D. Bohm and J. P. Vigier, "Model of the causal interpretation of quantum theory in terms of a fluid with irregular fluctuations," Phys. Rev. **96**, 208–216 (1954).
[21]J. Luck and A. Mehta, "Bouncing ball with a finite restitution: Chattering, locking, and chaos," Phys. Rev. E **48**, 3988 (1993).
[22]A. L. P. Livorati, T. Kroetz, C. P. Dettmann, I. L. Caldas, and E. D. Leonel, "Transition from normal to ballistic diffusion in a one-dimensional impact system," Phys. Rev. E **97**, 032205 (2018).
[23]A. U. Oza, D. M. Harris, R. R. Rosales, and J. W. M. Bush, "Pilot-wave dynamics in a rotating frame: On the emergence of orbital quantization," J. Fluid Mech. **744**, 404–429 (2014).
[24]M. Labousse, S. Perrard, Y. Couder, and E. Fort, "Self-attraction into spinning eigenstates of a mobile wave source by its emission back-reaction," Phys. Rev. E **94**, 042224 (2016).
[25]N. Sampara and T. Gilet, "Two-frequency forcing of droplet rebounds on a liquid bath," Phys. Rev. E **94**, 053112 (2016).
[26]N. Sungar, L. D. Tambasco, G. Pucci, P. J. Sáenz, and J. W. M. Bush, "Hydrodynamic analog of particle trapping with the Talbot effect," Phys. Rev. Fluids **2**, 103602 (2017).
[27]H. Talbot, "Facts relating to optical science," Philos. Mag. **9**, 401–407 (1836).
[28]R. Newell, J. Sebby, and T. G. Walker, "Dense atom clouds in a holographic atom trap," Opt. Lett. **28**, 1266–1268 (2003).
[29]Y. Y. Sun, X.-C. Yuan, L. S. Ong, J. Bu, S. W. Zhu, and R. Liu, "Large-scale optical traps on a chip for optical sorting," Appl. Phys. Lett. **90**, 031107 (2007).
[30]S. Protière, A. Boudaoud, and Y. Couder, "Particle-wave association on a fluid interface," J. Fluid Mech. **554**, 85–108 (2006).
[31]A. Eddi, D. Terwagne, E. Fort, and Y. Couder, "Wave propelled ratchets and drifting rafts," Europhys. Lett. **82**, 44001 (2008).
[32]J. Molácek and J. W. M. Bush, "Drops bouncing on a vibrating bath," J. Fluid Mech. **727**, 582–611 (2013).
[33]J. Molácek and J. W. M. Bush, "Drops walking on a vibrating bath: Towards a hydrodynamic pilot-wave theory," J. Fluid Mech. **727**, 612–647 (2013).
[34]P. Milewski, C. Galeano-Rios, A. Nachbin, and J. W. M. Bush, "Faraday pilot-wave dynamics: Modelling and computation," J. Fluid Mech. **778**, 361–388 (2015).
[35]D. M. Harris and J. W. Bush, "Generating uniaxial vibration with an electrodynamic shaker and external air bearing," J. Sound Vib. **334**, 255–269 (2015).
[36]S. Douady, "Experimental study of the Faraday instability," J. Fluid Mech. **221**, 383–409 (1990).
[37]B. A. Puthenveettil and E. J. Hopfinger, "Evolution and breaking of parametrically forced capillary waves in a circular cylinder," J. Fluid Mech. **633**, 355–379 (2009).
[38]C. L. Goodridge, W. T. Shi, H. G. E. Hentschel, and D. P. Lathrop, "Viscous effects in droplet-ejecting capillary waves," Phys. Rev. E **56**, 472–475 (1997).
[39]D. M. Harris, T. Liu, and J. W. M. Bush, "A low-cost, precise piezoelectric droplet-on-demand generator," Exp. Fluids **56**, 83 (2015).
[40]P. Flory, *Statistical Mechanics of Chain Molecules* (Interscience Publishers, 1969).
[41]T. Gilet, "Quantumlike statistics of deterministic wave-particle interactions in a circular cavity," Phys. Rev. E **93**, 042202 (2016).
[42]T. Gilet and J. W. M. Bush, "The fluid trampoline: Droplets bouncing on a soap film," J. Fluid Mech. **625**, 167–203 (2009).
[43]W. Zhang and J. Viñals, "Pattern formation in weakly damped parametric surface waves," J. Fluid Mech. **336**, 301–330 (1997).
[44]L. D. Tambasco and J. W. M. Bush, "Exploring orbital dynamics and trapping with a generalized pilot-wave framework," Chaos (submitted).
[45]M. Hubert, S. Perrard, M. Labousse, and N. Vandewalle,"Memory-driven run and tumble deterministic dynamics" e-print arXiv: 1807.02413.
[46]T. Gilet, "Dynamics and statistics of wave-particle interactions in a confined geometry," Phys. Rev. E **90**, 052917 (2014).
[47]L. E. Ballentine, "The statistical interpretation of quantum mechanics," Rev. Mod. Phys. **42**, 358–381 (1970).